View metadata, citation and similar papers at core.ac.uk
brought to you by CORE
provided by PolyU Institutional Repository

# Tilted fiber grating accelerometer incorporating an abrupt biconical taper for cladding to core recoupling

**Tuan Guo,[1,*] Liyang Shao,[1] Hwa-Yaw Tam,[1] Peter A. Krug[2] and Jacques Albert[2]**

[1]*Photonics Research Center, Department of Electrical Engineering, The Hong Kong Polytechnic University, Kowloon, Hong Kong SAR, China*

[2]*Department of Electronics, Carleton University, 1125 Colonel By Drive, Ottawa, Ontario K1S 5B6, Canada*

**guotuan2001@163.com*

**Abstract:** We demonstrate a compact power-referenced fiber-optic accelerometer using a weakly tilted fiber Bragg grating (TFBG) combined with an abrupt biconical taper. The electric-arc-heating induced taper is located a short distance upstream from the TFBG and functions as a bridge to recouple the TFBG-excited lower-order cladding modes back into the fiber core. This recoupling is extremely sensitive to microbending. We avoid complex wavelength interrogation by simply monitoring power change in reflection, which we show to be proportional to acceleration. In addition, the Bragg resonance is virtually unaffected by fiber bending and can be used as a power reference to cancel out any light source fluctuations. The proposed sensing configuration provides a constant linear response (nonlinearity < 1%) over a vibration frequency range from DC to 250 Hz. The upper vibration frequency limit of measurement is determined by mechanical resonance, and can be tuned by varying the sensor length. The tip-reflection sensing feature enables the sensor head to be made small enough (20~100 mm in length and 2 mm in diameter) for embedded detection. The polymer-tube-package makes the sensor sufficiently stiff for in-field acceleration measurement.

©2009 Optical Society of America

**OCIS codes:** (060.2370) Fiber optics sensors; (060.0060) Fiber optics and optical communications

## References and links

1. A. S. Gerges, T. P. Newson, J. D. C. Jones, and D. A. Jackson, "High-sensitivity fiber-optic accelerometer," Opt. Lett. **14**(4), 251–253 (1989).
2. S. T. Vohra, B. Danver, A. Tveten, and A. Dandridge, "High performance fibre optic accelerometers," Electron. Lett. **33**(2), 155–157 (1997).
3. C. Doyle, and G. F. Fernando, "Two-axis optical fiber accelerometer," Meas. Sci. Technol. **19**, 959–961 (2000).
4. G. A. Cranch, and P. J. Nash, "High-responsivity fiber-optic flexural disk accelerometers," J. Lightwave Technol. **18**(9), 1233–1243 (2000).
5. Y. J. Wang, H. Xiao, S. W. Zhang, F. Li, and Y. L. Liu, "Design of a fibre-optic disc accelerometer: theory and experiment," Meas. Sci. Technol. **18**(6), 1763–1767 (2007).
6. T. A. Berkoff, and A. D. Kersey, "Experimental demonstration of a fiber Bragg grating accelerometer," IEEE Photon. Technol. Lett. **8**(12), 1677–1679 (1996).
7. M. D. Todd, G. A. Johnson, B. A. Althouse, and S. T. Vohra, "Flexural beam-based fiber Bragg grating accelerometers," IEEE Photon. Technol. Lett. **10**(11), 1605–1607 (1998).
8. T. K. Gangopadhyay, "Prospects for fibre Bragg gratings and fabry-perot interferometers in fibre-optic vibration sensing," Sens. Actuators A Phys. **113**(1), 20–38 (2004).
9. A. Fender, W. N. MacPherson, R. R. J. Maier, J. S. Barton, D. S. George, R. I. Howden, G. W. Smith, B. J. S. Jones, S. McCulloch, X. F. Chen, R. Suo, L. Zhang, and I. Bennion, "Two-axis temperature-insensitive accelerometer based on multicore fiber Bragg gratings," IEEE Sens. J. **8**(7), 1292–1298 (2008).
10. Y. N. Zhu, P. Shum, C. Lu, M. B. Lacquet, P. L. Swart, and S. J. Spammer, "Temperature-insensitive fiber Bragg grating accelerometer," IEEE Photon. Technol. Lett. **15**(10), 1437–1439 (2003).
11. R. Romero, O. Frazão, D. A. Pereira, H. M. Salgado, F. M. Araújo, and L. A. Ferreira, "Intensity-referenced and temperature-independent curvature-sensing concept based on chirped fiber Bragg gratings," Appl. Opt. **44**(18), 3821–3826 (2005).

#117360 - $15.00 USD Received 17 Sep 2009; revised 14 Oct 2009; accepted 17 Oct 2009; published 26 Oct 2009

12. T. Guo, Q. D. Zhao, H. Zhang, C. S. Zhang, G. L. Huang, L. F. Xue, and X. Y. Dong, "Temperature-insensitive fiber Bragg grating dynamic pressure sensing system," Opt. Lett. **31**(15), 2269–2271 (2006).
13. T. Guo, A. Ivanov, C. Chen, and J. Albert, "Temperature-independent tilted fiber grating vibration sensor based on cladding-core recoupling," Opt. Lett. **33**(9), 1004–1006 (2008).
14. J. D. Love, W. M. Henry, W. J. Stewart, R. J. Black, S. Lacroix, and F. Gonthier, "Tapered single-mode fibres and devices Part 1: Adiabaticity criteria," IEE Proc.J. Optoelectron. **138**, 343–354 (1991).
15. R. J. Black, S. Lacroix, F. Gonthier, and J. D. Love, "Tapered single-mode fibres and devices Part 2: Experimental and theoretical quantification," IEE Proc.J. Optoelectron. **138**, 355–364 (1991).
16. E. C. Mägi, P. Steinvurzel, and B. J. Eggleton, "Tapered photonic crystal fibers," Opt. Express **12**(5), 776–784 (2004).
17. H. C. Nguyen, B. T. Kuhlmey, E. C. Magi, M. J. Steel, P. Domachuk, C. L. Smith, and B. J. Eggleton, "Tapered photonic crystal fibres: properties, characterisation and applications," Appl. Phys. B **81**(2-3), 377–387 (2005).
18. S. Laflamme, S. Lacroix, J. Bures, and X. Daxhelet, "Understanding power leakage in tapered solid core microstructured fibers," Opt. Express **15**(2), 387–396 (2007).
19. A. J. Fielding, K. Edinger, and C. C. Davis, "Experimental observation of mode evolution in single-mode tapered optical fibers," J. Lightwave Technol. **17**(9), 1649–1656 (1999).
20. O. Frazão, R. Falate, J. L. Fabris, J. L. Santos, L. A. Ferreira, and F. M. Araújo, "Optical inclinometer based on a single long-period fiber grating combined with a fused taper," Opt. Lett. **31**(20), 2960–2962 (2006).
21. O. Frazão, P. Caldas, F. M. Araújo, L. A. Ferreira, and J. L. Santos, "Optical flowmeter using a modal interferometer based on a single nonadiabatic fiber taper," Opt. Lett. **32**(14), 1974–1976 (2007).
22. Z. B. Tian, S. S. Yam, and H. P. Loock, "Refractive index sensor based on an abrupt taper Michelson interferometer in a single-mode fiber," Opt. Lett. **33**(10), 1105–1107 (2008).
23. D. Monzón-Hernández, V. P. Minkovich, J. Villatoro, M. P. Kreuzer, and G. Badenes, "Photonic crystal fiber microtaper supporting two selective higher-order modes with high sensitivity to gas molecules," Appl. Phys. Lett. **93**(8), 081106 (2008).
24. J. Ju, L. Ma, W. Jin, and Y. M. Hu, "Photonic bandgap fiber tapers and in-fiber interferometric sensors," Opt. Lett. **34**(12), 1861–1863 (2009).
25. R. T. Schermer, "Mode scalability in bent optical fibers," Opt. Express **15**(24), 15674–15701 (2007).
26. C. F. Chan, C. Chen, A. Jafari, A. Laronche, D. J. Thomson, and J. Albert, "Optical fiber refractometer using narrowband cladding-mode resonance shifts," Appl. Opt. **46**(7), 1142–1149 (2007).

## 1. Introduction

Structural health monitoring is a critical issue in various engineering applications, especially for large civil structures. Among many parameters to consider, vibration is one of the key measurements for monitoring structures. For more than two decades, fiber-optic accelerometers have attracted considerable interest for their unique properties. In many of the fiber-optic systems reported to date, measurement of acceleration is accomplished by simple inertial mass displacement that couples strain to a length of optical fiber, often configured in the form of fiber interferometer [1–5]. More recently, fiber Bragg grating (FBG) sensors have been proposed and demonstrated to provide quasi-static and dynamic strain measurements [6–9]. In these sensors, the recovery of the signal information is accomplished by the detection of the strain-induced wavelength changes of a FBG element. In order to simplify and reduce the cost of the interrogation scheme, some intensity-based studies have been performed for vibration and acceleration measurement, typically by the methods of nonuniform-strain induced FBG chirp modulation in specially designed cantilever beams [10–12]. However, one key downside of power-referenced sensing schemes is that they suffer from light source power fluctuations and therefore an additional power reference is needed for calibration. Also, cantilever-beam based accelerometers are difficult to fabricate and they are not suitable for embedding in engineered structures.

In this paper, we report on the design and performance of a compact tilted fiber Bragg grating (TFBG) accelerometer. The scheme is based on the recoupling of a set of low order wavelength-degenerate cladding modes known collectively as the "ghost" modes. These ghost modes are excited by the TFBG in the fiber core as described in our recent paper on an offset TFBG vibration sensor [13]. However, the current paper describes an alternative approach which takes advantage of lower orientation dependence and a better reproducibility in fabrication. Here, the recoupling occurs at an abrupt (i.e. non-adiabatic) biconical fused taper, in which the amount of recoupling is strongly dependent on fiber bend radius, thus providing the sensing mechanism. At the same time, the core-mode reflection from the same weakly tilted fiber Bragg grating is virtually unaffected by bending (lying, as it does, on the neutral strain axis of pure bending) and therefore the power reflected at the Bragg wavelength can be

#117360 - $15.00 USD Received 17 Sep 2009; revised 14 Oct 2009; accepted 17 Oct 2009; published 26 Oct 2009
(C) 2009 OSA

used as a power reference to cancel out any light source and transmission power level fluctuations. The sensor presents a linear acceleration response over a frequency range from DC to hundreds of Hz, covering the key frequencies to be measured for civil engineering structural monitoring (<10 Hz) and seismic measurements (< 20Hz, especially 2~3 Hz).

## 2. Sensor design and fabrication

Optical fibers with taper structures for core mode coupling in single- and multimode fibers and photonic crystal fibers [14–18] have been extensively studied. For such applications more gradual tapers with smaller taper angles are preferred, as they are focused largely on reducing the insertion loss by adiabatically tapering single-mode fiber to waist diameters of tens of micrometers. For larger taper angles or abrupt tapers, light in the core will be partially coupled into the cladding [19] and vice versa. Some taper-based fiber interferometers for sensing applications have been reported, typically combined with a long period grating (LPG) [20], assisted by a gold-coated fiber end for enhanced reflection [21,22] and based on photonic crystal fibers [23,24].

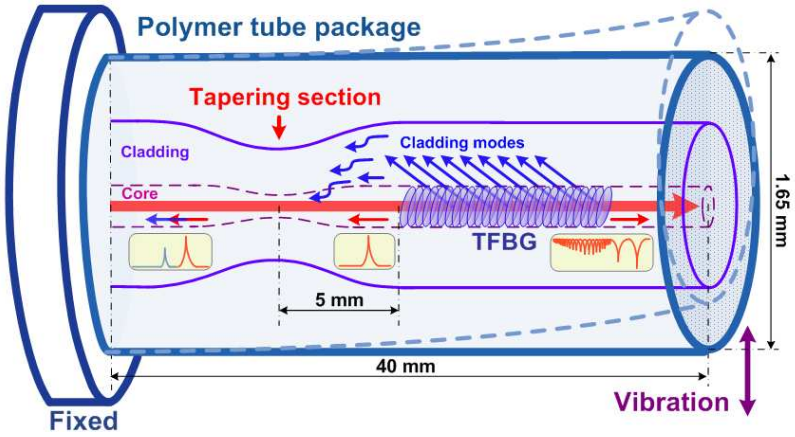


Fig. 1. Schematic diagram of abrupt-tapered TFBG accelerometer.

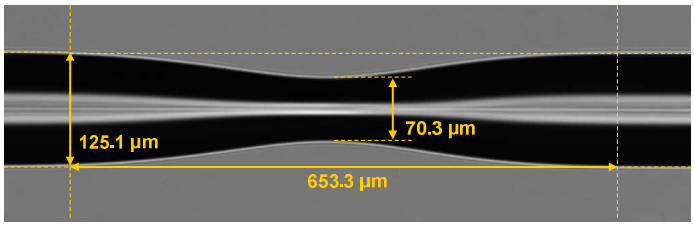


Fig. 2. Photograph of the electric-arc-heating induced abrupt-taper with a diameter waist of 70 μm over a length of 653 μm.

The sensor is shown schematically in Fig. 1. We used heating provided by an electric arc to fabricate an abrupt biconical taper in order to recouple part of TFBG excited cladding modes into the core so that they can propagate back to the interrogation system with low loss. The taper section was located at a point about 5 mm upstream from the TFBG and it was fabricated using a Vytran GPX-3400 glass processing system which incorporates a filament "furnace" assembly to provide a stable high-temperature heat source for precise control of fiber processing conditions. The heat source consists of an "omega" shaped tungsten resistive filament loop with a diameter of 900 μm and width of 625 μm. The filament loop was driven by electric current and the fiber inside can be heated to its softening point in a very repeatable and controllable manner. A single-mode fiber containing the TFBG was precisely positioned by two stepper-motor-controlled fiber holder blocks (FHBs) with an axial movement

#117360 - $15.00 USD Received 17 Sep 2009; revised 14 Oct 2009; accepted 17 Oct 2009; published 26 Oct 2009
(C) 2009 OSA

resolution of 0.25 μm. The filament power was 18 W with a heating duration of 3.2 seconds. During the heating process, the fiber was longitudinally stretched by the mechanical force exerted by the two FHBs on both sides in an opposite direction with a speed of 85 μm/s. As the microscope image of Fig. 2 shows, the combined effect of azimuthally uniform heating and sustaining axial tension created a symmetrical biconical taper with a waist diameter of 70 μm over an abrupt tapering length of 650 μm. In the figure we can see that the fiber core shows a slim tapered curve, similar to the outside cladding surface. As the low order cladding modes (particularly the ghost modes) are strongly confined near the internal core-cladding surface, we expect the taper to function as a bridge between core and cladding modes. Therefore, bending induced fluctuations in the reflected power of the low-order cladding modes can eventually be extracted from the upstream fiber core.

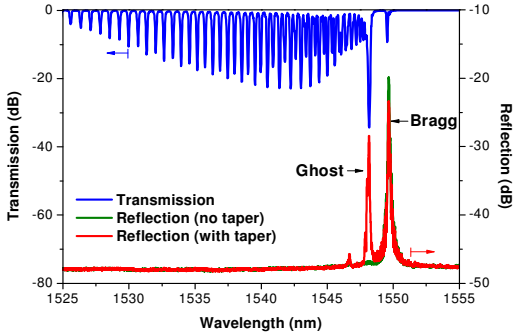


Fig. 3. TFBG spectra with and without taper.

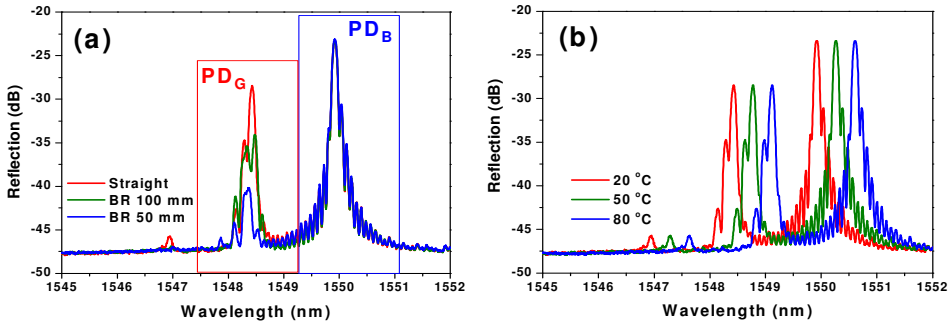


Fig. 4. Tapered TFBG reflection spectra versus (a) bending and (b) temperature.

Once the reflected cladding modes are recoupled into the fiber core, they can propagate over a long distance with a transmission loss as low as that of the core mode. As Fig. 3 shows, compared with the original TFBG reflection (green curve), the TFBG plus taper reflection (red curve) then consists of a strongly recoupled ghost resonance on the shorter wavelength side and the Bragg resonance, which is attenuated by about 3 dB due to loss in the taper. Bending the fiber introduces changes of the transverse intensity distribution of the mode [25], and reduces the recoupling efficiency from the backward transmitted cladding modes to the core of the interrogating fiber. Therefore the recoupled low-order cladding modes show an extremely high sensitivity to fiber bending. Figures 4(a) and 4(b) show how the reflection spectra change with bend radius (BR) and temperature perturbations, respectively. Apart from an 11.5 pm/°C shift, as shown in Fig. 4(b), their spectral shapes are invariant with temperature. However, changing the bend radius from infinity to 50 mm results in more than 10 dB of reduction of the recoupled ghost mode power but no visible change in the core mode reflection. It should be further mentioned that the low order cladding modes used here are well confined near the fiber axis and essentially insensitive to the refractive index of the medium that surrounds the fiber [26]. Therefore, the bare fiber-taper tip can be coated with a

#117360 - $15.00 USD Received 17 Sep 2009; revised 14 Oct 2009; accepted 17 Oct 2009; published 26 Oct 2009
(C) 2009 OSA

protective coating and/or embedded into a package with any bonding material without fear of modifying the optical response.

To gain a better understanding of the characteristics of the ghost modes we used numerical mode simulation (OptiGrating) to analyze the composition of the ghost resonance and the transverse electric field amplitude distributions of its constituent modes. We modeled the modes of a TFBG with a 4° tilt angle and Bragg resonance centered at 1550 nm. Among low order $LP_{nm}$ modes (n = 0 to 3) we found that the first order odd $LP_{1m}$ modes with m = 1 to 4 contribute most to the ghost resonance. Figure 5 shows the amplitude distributions and transmission spectra of the basic low order cladding $LP_{nm}$ modes and the first-order odd $LP_{1m}$ modes which contribute most to the ghost resonance (the red curves of the inset in Fig. 5). Because these first-order odd modes are adjacent to the core-cladding interface with an asymmetrical distribution, any slight fiber bending may induce a change in their transverse electric field amplitude distributions. Consequently, the recoupling efficiency at the taper junction is strongly modulated, providing a highly sensitive fiber-optic accelerometer. Although the combined spectrum of the resonances making up the ghost resonance is complicated and irregular, it does not matter as we are measuring the total power in the spectral band covering the whole resonance, not the detailed spectral shape.

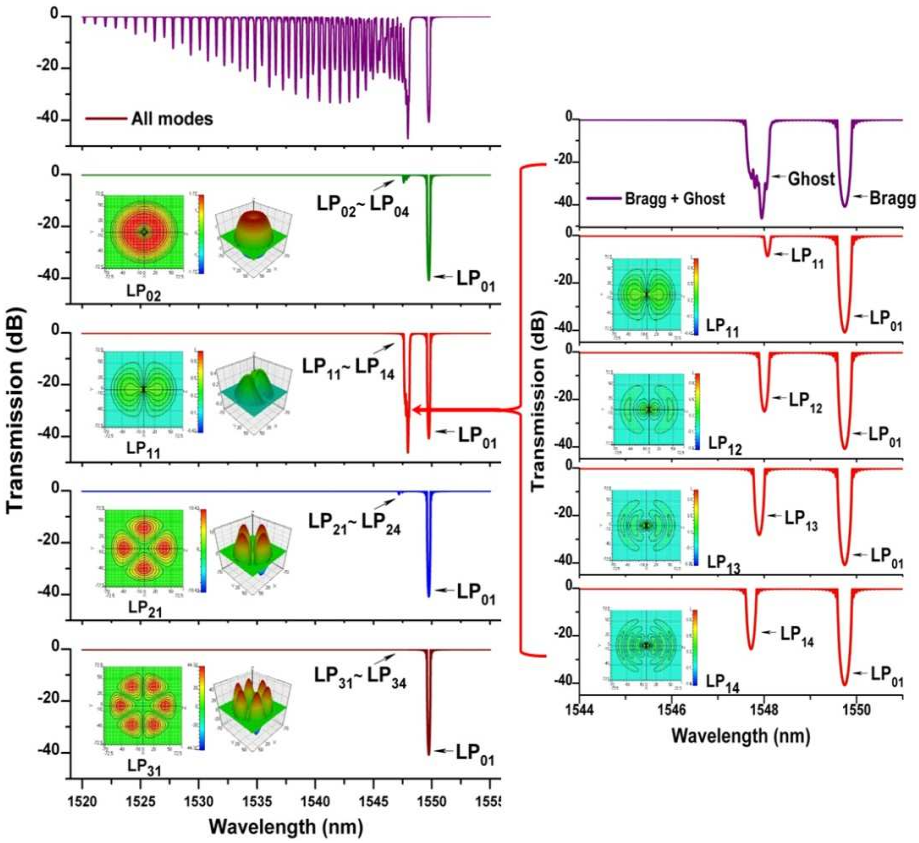


Fig. 5. Numerical analysis of the composition of the ghost modes in a 4° TFBG: the amplitude distributions and transmission spectra of the basic low order cladding LPnm modes and the first-order odd LP1m modes (inset).

## 3. Experiment and discussion

Figure 6 shows the experimental setup of the acceleration sensing system. The accelerometer can be functionally divided into two parts: the supporting aluminum box and the polymer tube

#117360 - $15.00 USD Received 17 Sep 2009; revised 14 Oct 2009; accepted 17 Oct 2009; published 26 Oct 2009
(C) 2009 OSA

which serves as the package of the sensing grating and taper. A commercial piezoelectric accelerometer attached above the box lid is used for calibration. A 10-mm long, 4° tilted grating was inscribed in hydrogen-loaded Corning SMF-28 fiber using a pulsed KrF excimer laser and the phase mask technique. A fiber section containing the taper and TFBG was cleaved a few mm downstream from the taper and packaged inside a polymer tube with an outside diameter of 1.65 mm and wall thickness of 0.5 mm. The space inside the tube, surrounding the fiber was filled with UV-curing epoxy acrylate adhesive to ensure that the tilted FBG senses the vibration of the composite structure which consists of the polymer tube, the tilted FBG and the fully cured, rigid epoxy acrylate. The polymer tube was clamped at one end and free on the other end. Light from a broadband source was launched into the TFBG sensor through a 3 dB coupler and the reflected spectrum was monitored with an optical spectrum analyzer with a spectral resolution of 0.05 nm. The reflected power of the core mode and cladding modes were monitored by two photodiodes via a 2-nm bandwidth bandpass filter in each photodetector. The optical bandpass filters are centered on the recoupled ghost and Bragg resonances near 1548 nm and 1550 nm, respectively, as shown in Fig. 4(a).

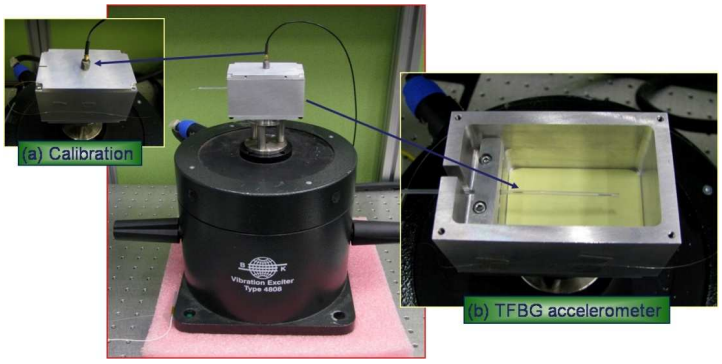


Fig. 6. Experimental setup of the acceleration sensing system (centre), with insets of (a) acceleration calibration and (b) polymer tube sensing configuration.

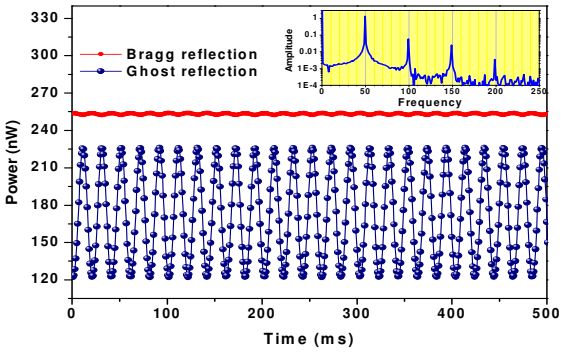


Fig. 7. Power response of Bragg & ghost reflection of sensor with a tube length of 32 mm and following a harmonic oscillation (~50 Hz) as inset.

### *3.1 Linear responsivity*

The blue curve in Fig. 7 presents the bandpass-filtered reflected power of the ghost resonance in response to a 50 Hz harmonic oscillation. The red curve in Fig. 7 shows the corresponding response of the Bragg resonance: the reflected power in the Bragg resonance band remains relatively constant ( ± 1 nW) compared to the ± 52 nW perturbation of the ghost response. We use peak-to-peak power amplitude of the ghost resonance as the sensor output. Experimental tests show that, the sensor demonstrates extremely linear response of the detected peak-to-

#117360 - $15.00 USD Received 17 Sep 2009; revised 14 Oct 2009; accepted 17 Oct 2009; published 26 Oct 2009
(C) 2009 OSA

peak power output ($P_{p-p}$) versus applied acceleration (in units of G = 9.8 m/s$^2$), as shown in Fig. 8 for the 40 Hz harmonic oscillation output of sensor with a resonant frequency of 82 Hz.

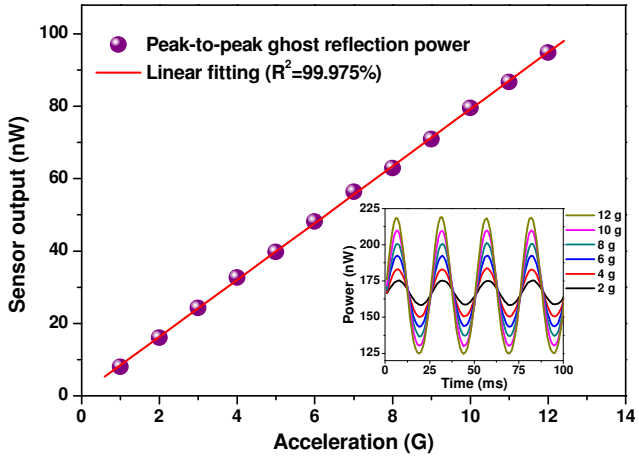


Fig. 8. Linear response of sensor output ($P_{p-p}$) versus applied acceleration (G). The inset shows ghost power response in time domain (40 Hz harmonic oscillation output for the sensor with a resonant frequency of 82 Hz).

*3.2 Flat response over a broad frequency range*

From a practical point of view, it is important that vibration sensors have a flat response over a range of acoustic frequencies. We investigated the acceleration responsivity of the sensor over a broad vibration frequency range. Figure 9 shows the frequency response of the sensor for three sensor tube lengths. For each length, there is a flat response at frequencies less than the mechanical resonance frequency. For frequencies larger than the resonance frequency, the response falls quickly to zero. Clearly, there is a trade-off between the frequency range and the responsivity of the sensor. The inset in Fig. 9 shows the decrease in non-resonant response of the sensor as the frequency is increased from DC to 250 Hz.

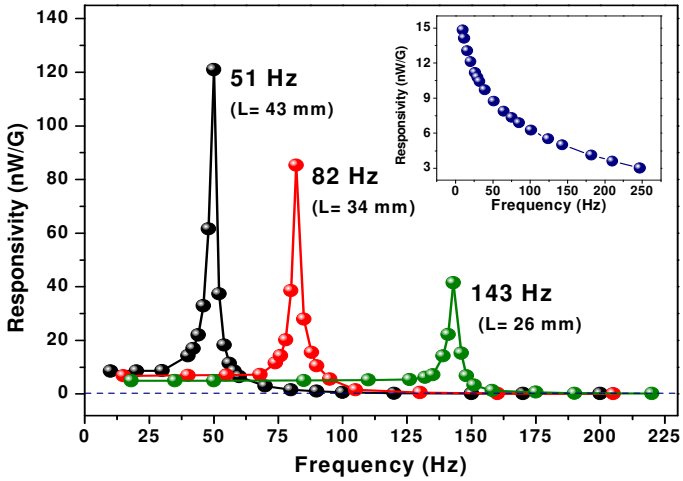


Fig. 9. Acceleration responsivity of sensor tubes with different free length over a broad frequency.

#117360 - $15.00 USD Received 17 Sep 2009; revised 14 Oct 2009; accepted 17 Oct 2009; published 26 Oct 2009
(C) 2009 OSA

*3.3 Adjustable resonance frequency*

The resonance frequency of a cantilevered beam is given by:

$$f = \frac{1}{2\pi}\sqrt{\frac{8EI}{\rho A l^4}} \tag{1}$$

where $E$ is Young's modulus of the beam, $I$ is the moment of inertia of the beam about the pivot, $\rho$ is the density of the beam, $A$ is the cross-sectional area of the beam and $l$ is the length of the beam. From Eq. (1), we can see that the resonant frequency can be increased by increasing the stiffness (effective Young's modulus for the complete assembly), or by reducing the effective density, cross-sectional area or length of the sensor. Changing any of these parameters will result in a shift of resonant frequency of the sensor. However, the effect of $l$ is the parameter to which the resonant frequency is most sensitive and the easiest adjustable parameter for practical applications. For a cylindrical beam, $A = \pi r^2$, where $r$ is the radius of the beam, and $I = \pi r^4 / 4$. For example, a bare fiber clamped at one end, with $l$ = 43 mm, $r$ = 62.5 μm, and assuming the density and Young's modulus of fused silica are 2650 kg/m$^2$ and 73 GPa, respectively, has a resonant frequency $f$ = 40 Hz. However, if we package the fiber with polyethylene encapsulated polymer tube, the resonant frequency is dominated by the packaging materials rather than the glass fiber. Here the polymer tube is polyvinyl chloride (PVC, with a Young's modulus of 1.5 GPa) and the adhesive used is epoxy acrylate (with a Young's modulus of 0.2 GPa). If the effective Young's modulus is 0.66 GPa, then for a 43-mm long tube of radius 0.83 mm, the calculated resonant frequency is around 50 Hz which is in good agreement with our experimental resonant peak of 51 Hz. Equation (1) predicts that $f \propto 1/l^2$. This relation was confirmed experimentally by measuring the resonant frequency of the sensor with the tube clamped at various distances from its free end. The results are shown in Fig. 10.

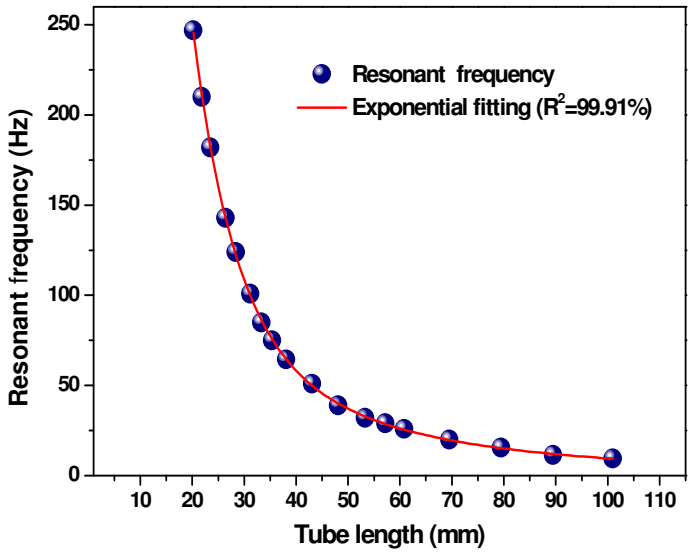


Fig. 10. Resonant frequency of the accelerometer tube (d = 1.65 mm) versus its free length, combining with a calculated exponential fitting of f = 110058/l$^{-2}$ (red curve).

#117360 - $15.00 USD Received 17 Sep 2009; revised 14 Oct 2009; accepted 17 Oct 2009; published 26 Oct 2009
(C) 2009 OSA

*3.4 Angular dependence*

The fiber grating is known to display orientation sensitivity because of the directionality of the grating writing process. A related issue is the sensitivity of the responsivity to the angle between the plane of vibration and the tilt of the grating. This is quite an important question in any application where the direction of the vibration is not predetermined. We measured the angular dependence of sensor responsivity as the sensor was rotated relative to the direction of the vibration. The results are displayed in Fig. 11. The responsivity presents an asymmetrical figure-of-eight-shaped curve, with peak relative sensitivity of 1 and 0.65 at 90° and 270°, respectively. The non-zero minima in the sensor response at 0° and 180° indicate that the sensor still has a certain degree of perpendicular sensitivity. It should be emphasized that the difference between two peak sensitivities at 90° and 270° is mainly due to an unwanted slight pre-bending of the polymer tube which is induced by the solidifying of encapsulated UV-curing glue. In our experimental setup, the plane of vibration was vertical. Gravity biases the response and this results in the asymmetry in the response at 90° and 270° that we see in Fig. 11. Otherwise, the sensor is expected to be totally insensitive to rotation by 180° under a harmonic sinusoidal vibration.

Beside the strong directionality of the grating tilt and as-fabricated slight bend in the packaged sensor, there are still two potential orientation-sensitive factors should be considered. One is the cladding-to-core recoupling efficiency at the taper junction and the other is the possible laterally offset from the neutral axis of the assembly when mounting the fiber in its tubular housing. To achieve a controllable angular dependence and a better reproducibility, the aforementioned two orientation-dependences should be minimized. We use the biconical taper instead of the previously reported lateral-offset splice as a means to recouple cladding modes into the core [13], because the “omega” shaped heat source (tungsten resistive filament loop) provides cylindrically symmetrical heating and therefore decreases the angular dependence of the taper section. Even using a conventional arc discharge fiber splicer can induce a smooth taper curve with low internal orientation-dependence. Next we consider the second aspect of the potential non axial packaging. Because the internal diameter of tube (~1 mm) is quite small compared to its length (20-100 mm) and the fiber inside it supported by encapsulating adhesive, the orientation-sensitivity arising from this effect is small. However, in the case of a larger diameter tube assembly, nonaxial packaging will induce additional stretching and compression as the fiber bent, which potentially could enhance the sensitivity.

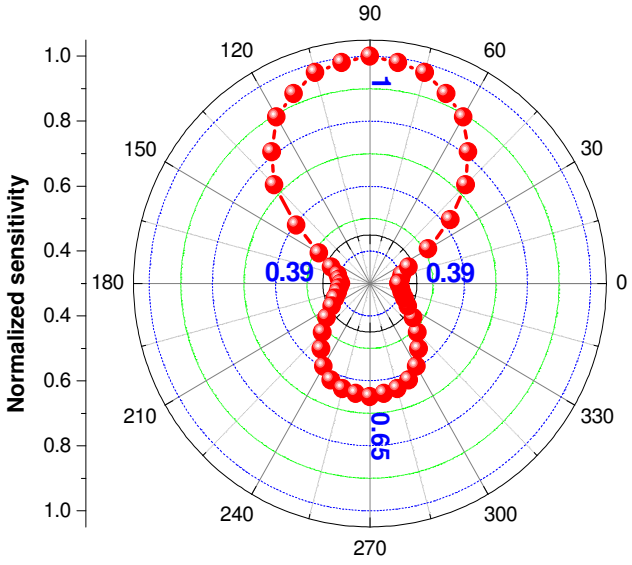


Fig. 11. Angular dependence of acceleration responsivity.

#117360 - $15.00 USD Received 17 Sep 2009; revised 14 Oct 2009; accepted 17 Oct 2009; published 26 Oct 2009
(C) 2009 OSA

## 4. Conclusion

We have presented a fiber-optic accelerometer comprising a tilted fiber Bragg grating and an abrupt biconical taper, all encapsulated in a plastic tube using a rigid ultraviolet-cured acrylate epoxy. The composite structure is very stiff to ensure a good transfer of the vibrations from the tube to the tilted FBG and provides long term protection, even in harsh environments. Appropriate design considerations have resulted in an accelerometer with the following desirable features: (i) less than 1% deviation from linearity of response over an acceleration range from 0.5 to 12.5 G, (ii) flat response over a vibration frequency range from DC to 250 Hz, (iii) adjustable resonance frequency (dominated by the tube length), (iv) angular dependence (strong vibration-orientation sensitivity), (v) cost-effective interrogation (we measure power rather than wavelength), (vi) self-calibration (a spectrally separated Bragg resonance which is immune to vibration), and (vii) compact size (20~100 mm in length and diameter less than 2 mm, comparable to most commercially available accelerometer apart from the smallest MEMS based devices that have volumes of the order of $mm^3$). Our device is aimed at applications where optical sensors are preferred over electrical ones, for example, long term structural health monitoring of relatively large structures where a number of sensors need to be embedded and connected, or for applications where immunity to electromagnetic interference is critical (inside engines, for instance). For most of these applications, the frequency range demonstrated is more than sufficient. With regards to sensitivity, we have not attempted to increase it (by adding a small mass to the end of the sensor for instance) as this parameter is highly dependent on the application. Finally, in contrast to most currently developed fiber optic accelerometers the fiber needs no stretching to detect the acceleration, only large radius bending along its neutral axis, and the whole fiber can be embedded into a solid matrix. This will help to ensure the long-term reliability of our devices in real applications.

## Acknowledgments

The authors acknowledge support by the Central Research Grant of The Hong Kong Polytechnic University of Hong Kong Special Administrative Region, China (Project No. G-YX0W), support from the Natural Sciences and Engineering Research Council of Canada, the Canada Foundation for Innovation, and LxDATA (formerly LxSix Photonics). The authors acknowledge Mr. C. Champagne for helpful discussions. Prof. J. Albert acknowledges support from the Canada Research Chair Program.

#117360 - $15.00 USD Received 17 Sep 2009; revised 14 Oct 2009; accepted 17 Oct 2009; published 26 Oct 2009
(C) 2009 OSA